We are IntechOpen, the world's leading publisher of Open Access books Built by scientists, for scientists

6,900
Open access books available

185,000
International authors and editors

200M
Downloads

Our authors are among the

154
Countries delivered to

TOP 1%
most cited scientists

12.2%
Contributors from top 500 universities



WEB OF SCIENCE™

Selection of our books indexed in the Book Citation Index in Web of Science™ Core Collection (BKCI)

Interested in publishing with us?
Contact book.department@intechopen.com

Numbers displayed above are based on latest data collected.
For more information visit www.intechopen.com



1

Fourier Series and Fourier Transform with Applications in Nanomaterials Structure

Florica Matei[1] and Nicolae Aldea[2]
[1]*University of Agricultural Science and Veterinary Medicine, Cluj-Napoca,*
[2]*National Institute for Research and Development of Isotopic and Molecular Technologies, Cluj-Napoca,*
Romania

1. Introduction

One of the most important problems in the physics and chemistry of the nanostructured materials consists in the local and the global structure determination by X-ray diffraction and X-ray absorption spectroscopy methods. This contribution is dedicated to the applications of the Fourier series and Fourier transform as important tools in the determination of the nanomaterials structure. The structure investigation of the nanostructured materials require the understanding of the mathematical concepts regarding the Fourier series and Fourier transform presented here without theirs proofs. The Fourier series is the traditional tool dedicated to the composition of the periodical signals and its decomposition in discreet harmonics as well as for the solving of the differential equations. Whereas the Fourier transform is more appropriate tool in the study of the non periodical signals and for the solving of the first kind integral equations. From physical point of view the Fourier series are used to describe the model of the global structure of nanostructured materials that consist in: average crystallite size, microstrain of the lattice and distribution functions of the crystallites and microstrain versus size. Whereas the model for the local structure of the nanomaterials involves the direct and inverse Fourier transform. The information obtained consist in the number of atoms from each coordination shell and their radial distances.

2. Fourier series and theirs applications

One of the most often model studied in physics is the one of oscillatory movement of a material point. The oscillation of the electrical charge into an electrical field, the vibration of a tuning fork that generated sound waves or the electronic vibration into atoms that generate light waves are studied in the same mode (Richard et al., 2005). The motion equations related to the above phenomena have similar form; therefore the phenomena treated are analogous. From mathematical point of view these are modeled by the ordinary differential equations, most of them with constant coefficients. Due to the particular form of the equation any linear combination of the solution it is also a solution and the mathematical substantiation is given by the superposition principle. It consists in, if u_1, u_2, …, u_k are

solutions for the homogenous linear equations $L[u]=0$, then the linear combination (or the superposition) is a solution of $L[u]=0$ for any choice of the constants. The previous statement shows that the general solution of a linear equation is a superposition of its linearly independent particularly solution that compose a base in the finite dimension space of the solution. The superposition is true for any algebraic equations as well as any homogenous linear ordinary differential equations.

2.1 Physical concept and mathematical background

The analysis of the linear harmonic oscillatory motion for a material point of mass m round about equilibrium position due to an elastically force F=-Kx it is given by the harmonic equation that is a differential equations which appear very frequently in the analysis of physical phenomena (Tang, 2007)

$$m\frac{d^2x}{dt^2}+Kx=0 \tag{1}$$

with the solution $x(t)=A\cos(2\pi f_0 t-\varphi_0)$ where A, K, f_0, $\omega=\sqrt{\frac{K}{m}}$, $\omega=2\pi f_0$ and φ_0 represent the motion's amplitude, elastic constant, fundamental frequency, angular speed and phase shift, respectively. Generalizing let consider the physical signal given by

$$x(t)=\underbrace{a_1\sin(2\pi f_0 t)}_{f_0\ line}+\underbrace{a_2\sin(4\pi f_0 t)}_{2f_0\ line}+\underbrace{a_3\sin(6\pi f_0 t)}_{3f_0\ line}+\ldots+\underbrace{a_n\sin(2\pi n f_0 t)}_{nf_0\ line} \tag{2}$$

that is periodic but non harmonic process, the physical signal being a synthesis of n spectral lines with the frequencies f_0, $2f_0$, $3f_0$, …, nf_0 and the amplitudes $a_1, a_2, \ldots, a_n$, respectively. The practical problem that had lead to Fourier series was to solve the heat equation which is a parabolic partial differential equation. Before the Fourier contribution no solution for the general form of the heat equation was known. The Fourier idea was to consider the solution as a linear combination of sine or cosine waves in according with the superposition principle. The solution space for of the partial differential equation are infinite dimensional spaces thus there are needed an infinite number of independent solutions. Therefore is not possible to find all independent particular solutions of a linear partial differential equations. The key found by Joseph Fourier in his article "Théorie analitique de la chaleur", published in 1811, was to form a series with the basic solutions. The ortonormality is the key concept of the Fourier analysis. The general representation of the Fourier series with coefficients a, b_n and c_n is given by:

$$x(t)=\frac{a}{2}+\sum_{n=1}^{\infty}\left[b_n\cos(nt)+c_n\sin(nt)\right] \tag{3}$$

The Fourier series are used in the study of periodical movements, acoustics, electrodynamics, optics, thermodynamics and especially in physical spectroscopy as well as in fingerprints recognition and many other technical domains. It was proved (Walker, 1996) that any physical signal of the period T=1/f_0 can be represented as an harmonic function with the frequencies f_0, $2f_0$, $3f_0$, …

$$x(t) = \frac{a}{2} + \sum_{n=1}^{\infty} \left[b_n \cos(2\pi n f_0 t) + c_n \sin(2\pi n f_0 t) \right] \tag{4}$$

The Fourier coefficients are obtained in the following way:

i. by integration of the previous relation between $[-T/2, T/2]$

$$a = \frac{2}{T} \int_{-T/2}^{T/2} x(t) dt \tag{5}$$

ii. by multiplication of (4) with $\cos(2\pi n f_0 t)$ and integration

$$b_n = \frac{2}{T} \int_{-T/2}^{T/2} x(t) \cos(2\pi n f_0 t) dt \tag{6}$$

iii. by multiplication of (4) with $\sin(2\pi n f_0 t)$ and integration

$$c_n = \frac{2}{T} \int_{-T/2}^{T/2} x(t) \sin(2\pi n f_0 t) dt \tag{7}$$

Some observations about physical signal modeled by Fourier series are given below.

i. Value $a/2$ represents the mean value for the physical signal on $[-T/2, T/2]$.
ii. If $x(t + T/2) = -x(t)$ then Fourier series of x has only amplitudes with odd index (Tang, 2007) all the other terms will vanish:

$$x(t) = \sum_{n=0}^{\infty} \left[b_{2n+1} \cos(2\pi n f_0 t) + c_n \sin(2\pi n f_0 t) \right] \tag{8}$$

iii. In practice the argument of the function x can be a scalar as time, frequency, length, angle, and so on, thus (4) is defined on period [0, T], spectral interval [0,f], spatial interval $[0, L]$, wave length [0, λ] or the whole trigonometric circle, respectively.
iv. Using the Fourier coefficients the Parseval's equality is given by

$$\begin{aligned} \int_{-T/2}^{T/2} x^2(t)\, dt &= \int_{-T/2}^{T/2} x(t) \left\{ \frac{a}{2} + \sum_{n=1}^{\infty} \left[b_n \cos(2\pi n f_0 t) + c_n \sin(2\pi n f_0 t) \right] \right\} dt = \\ &= \frac{T}{2} \left[\frac{a^2}{2} + \sum_{n=1}^{\infty} \left(b_n^2 + c_n^2 \right) \right] \end{aligned} \tag{9}$$

The right term of the above equality represents the energy density of the signal x. Thus the Parseval equality shows that the whole density energy is contained in the squares of the all amplitudes of harmonic terms defined on the interval $[-T/2, T/2]$. The Parseval equality holds for any function whose square is integrable. The next problem is to analyze the convergence of the series. Because the aim of this chapter are the application of the Fourier series it will be only mentioned the basic principles of the Fourier analysis. If the interval $[-T/2, T/2]$ can be decomposed in a finite number of intervals on that the function f is

continuous and monotonic, then the function *f* has a Fourier series representation. The next consideration is connected with the $L^2[A,B]$ space defined below

$$L^2[A,B]=\left\{x:[A,B]\to R\left|\int_A^B |x(t)|^2\,dt<\infty\right.\right\} \tag{10}$$

The complete system for the $L^2[A,B]$ is given by

$$\begin{gathered}\sqrt{\frac{2}{B-A}},\sqrt{\frac{2}{B-A}}\cos\frac{2\pi t}{B-A},\sqrt{\frac{2}{B-A}}\sin\frac{2\pi t}{B-A},\cdots,\\ \sqrt{\frac{2}{B-A}}\cos\frac{2\pi kt}{B-A},\sqrt{\frac{2}{B-A}}\sin\frac{2\pi kt}{B-A},\cdots\end{gathered} \tag{11}$$

then any function from $L^2[A,B]$ can be written as a linear combination of its complete system and the Fourier coefficients are

$$\begin{gathered}a=\sqrt{\frac{2}{B-A}}\int_A^B x(t)dt,\\ \beta_k=\sqrt{\frac{2}{B-A}}\int_A^B x(t)\cos\frac{2\pi kt}{B-A}dt,\quad \gamma_k=\sqrt{\frac{2}{B-A}}\int_A^B x(t)\sin\frac{2\pi kt}{B-A}dt.\end{gathered} \tag{12}$$

2.2 Trigonometric polynomials and Fourier coefficients determination

One of the useful mathematical tools in order to apply the Fourier series in data analysis is the trigonometric polynomial. From physical point of view the trigonometric polynomials are used to characterize the periodic signals. The general form of the real trigonometric polynomial of degree *M* is given by:

$$P(t)=\frac{\alpha}{2}+\sum_{k=1}^{M}\left(\beta_k\cos\left(\frac{2\pi kt}{T}\right)+\gamma_k\sin\left(\frac{2\pi kt}{T}\right)\right) \tag{13}$$

where α, β_k, γ_k, T being real constants. Let denote by *S* the square deviation of the function *x* from trigonometric polynomial *P* defined on interval of length *T*

$$S(\alpha,\beta_1,\cdots,\beta_M,\gamma_1,\cdots,\gamma_M)=\int_{-T/2}^{T/2}\left(x(t)-P(t)\right)^2dt \tag{14}$$

Let enumerate some properties of trigonometric polynomials that will be used in this chapter (Bachmann et al., 2002).

i. Let *x* be a function in $L^2[-T/2,T/2]$, then from all polynomials of degree *M* the minimum of the square deviation is obtained for the trigonometric polynomial with the coefficient equal with the Fourier coefficients of function *x*;
ii. If the physical signal is defined on an arbitrary interval $[A,B]$ with period *B-A* then the trigonometric polynomial associated is given by

$$P(t)=\frac{\alpha}{2}+\sum_{k=1}^{M}\left(\beta_k\cos\left(\frac{2\pi kt}{B-A}\right)+\gamma_k\sin\left(\frac{2\pi kt}{B-A}\right)\right); \tag{15}$$

iii. The Fourier coefficients associated to polynomial P are obtained by the least square method and the linear system is

$$\begin{cases}\dfrac{\alpha}{2}\displaystyle\int_A^B dt+\sum_{K=1}^{M}\left\{\int_A^B\left[\beta_k\cos C_k-\gamma_k\sin C_k\right]dt\right\}=\int_A^B Y(t)dt\\ \dfrac{\alpha}{2}\displaystyle\int_A^B \cos C_m dt+\sum_{K=1}^{M}\left\{\int_A^B\left[\beta_k\cos C_k-\gamma_k\sin C_k\right]\cos C_m dt\right\}=\int_A^B Y(t)\cos C_m dt\\ \dfrac{\alpha}{2}\displaystyle\int_A^B \sin C_m dt+\sum_{K=1}^{M}\left\{\int_A^B\left[\beta_k\cos C_k-\gamma_k\sin C_k\right]\sin C_m dt\right\}=\int_A^B Y(t)\sin C_m dt\end{cases} \tag{16}$$

where $C_k=Ckt$, $C_m=Cmt$, $C=2\pi/(B-A)$, Y is the approximated function by the trigonometric polynomial of degree M and m =1, …, M. The system (16) has 2M+1 equations and due to the orthogonality properties of the functions $\cos C_k$ and $\sin C_k$ the solution of system (16) is

$$\alpha=\frac{2}{B-A}\int_A^B Y(t)dt,\ \beta_k=\frac{2}{B-A}\int_A^B Y(t)\cos\frac{2\pi kt}{B-A}dt \text{ and } \gamma_k=\frac{2}{B-A}\int_A^B Y(t)\sin\frac{2\pi kt}{B-A}dt; \tag{17}$$

iv. Previous considerations are often used in the process of global approximation of the discreet physical signals. Let consider the sequence of experimental values $(y_k,P_k)_{k=\overline{1,N}}$, with discretization step defined by $\Delta t=(B-A)/(N-1)$ thus $t_k=A+(k-1)\Delta t$ and then the approximate values of Fourier coefficients are given by

$$\begin{aligned}&\alpha\approx\frac{2}{N-1}\sum_{k=1}^{N}P_k\quad \beta_j\approx\frac{2}{N-1}\sum_{k=1}^{N}\left[P_k\cos\left(\frac{2\pi jA}{B-A}+\frac{2\pi j(k-1)}{N-1}\right)\right]\\ &\gamma_j\approx\frac{2}{N-1}\sum_{k=1}^{N}\left[P_k\sin\left(\frac{2\pi jA}{B-A}+\frac{2\pi j(k-1)}{N-1}\right)\right],\quad j=\overline{1,M};\end{aligned} \tag{18}$$

v. If the trigonometric polynomial pass through all the experimental points, that is

$$\begin{aligned}&P(t_i)=Y(t_i)\quad\Leftrightarrow\\ &\frac{\alpha}{2}+\sum_{k=1}^{M}\left(\beta_k\cos Cky_i+\gamma_k\sin Cky_i\right)=Y_i,\quad i=\overline{1..N}\end{aligned} \tag{19}$$

The system (16) is equivalent with $\sum_{i=1}^{N}\left(P(t_i)-Y_i\right)^2=0$ and represents the same condition find in the least squares method for the discreet case. The coefficients are given by (17) relations. In this case the degree of the trigonometric polynomial, M, has to satisfy the relation 2M+1=N where N represents the number of experimental points;

vi. The degree of approximation is given by the residual index defined by

$$R = 100\sum_{i=1}^{N}\frac{\left|y_i^{\exp} - P_i\right|}{y_i^{\exp}} \tag{20}$$

where $y_i^{\exp}$ represents the sequence of experimental values;

vii. The first derivative of the physical signal approximated by the trigonometric polynomial is given by

$$\frac{dP(t)}{dt} \approx -\frac{2\pi}{B-A}\sum_{i=1}^{M}\left(k\beta_k \sin\frac{2\pi kt}{B-A} - k\gamma_k \cos\frac{2\pi kt}{B-A}\right) \tag{21}$$

Previous relation can be useful only when the physical signal is less affected by the noise;

viii. Other application of the trigonometric polynomials is the determination of the integral intensity, *I*, of the physical signal

$$I \approx \frac{\alpha}{2}(B-A). \tag{22}$$

2.3 Application of the Fourier series in X-ray diffraction

The spectrum for X-ray diffraction for the nickel foil is represented in Fig.1. It has been registered with the Huber goniometer that used an incident fascicle with synchrotron radiation with the wavelength 1.8276 Å. The experimental data was recorded with constant step $\Delta\theta = 0.033^0$ and its number of pairs is n=766.

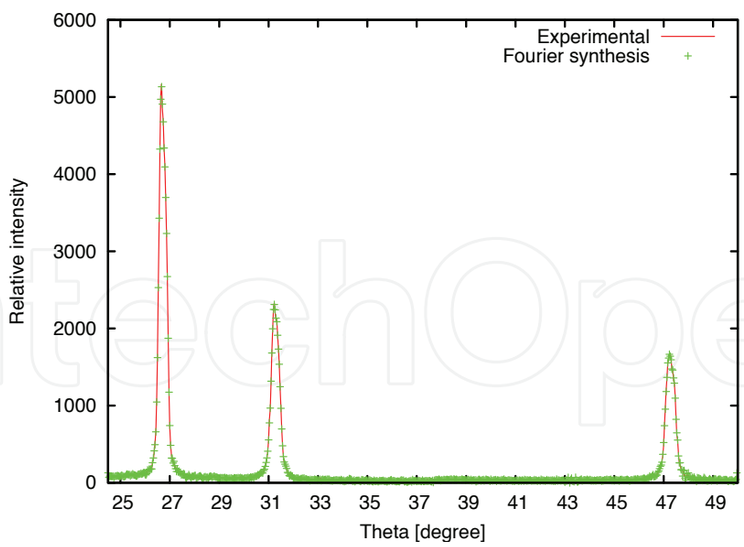


Fig. 1. Experimental spectrum of the nickel foil

The Miller indexes of the X-ray line profiles measurements are (111), (200), respectively (220). Data analysis of the experimental spectrum was realized by our package program (Aldea & Indrea, 1990). The Fig. 2 shows the square magnitude of Fourier coefficients versus the harmonic indexes. They are used in the Warren – Averbach model (Warren, 1990) for the

average crystallite size, microstrains of the lattice, total probability of the defaults and the distribution functions of the crystallites and the microstrains determination.

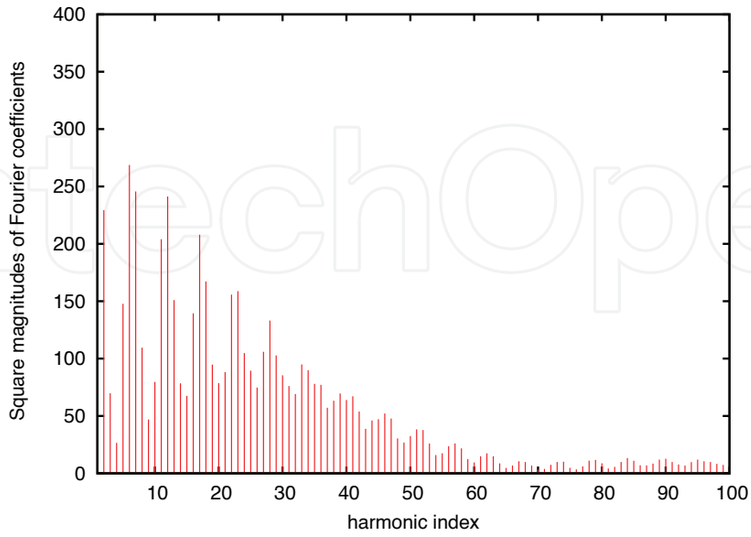


Fig. 2. The square magnitudes of the Fourier coefficients

The broadening of X-ray line profiles can be determined from the first derivative of the experimental spectrum analysis. The first derivative of the nickel foil spectrum in Fig. 3 is given.

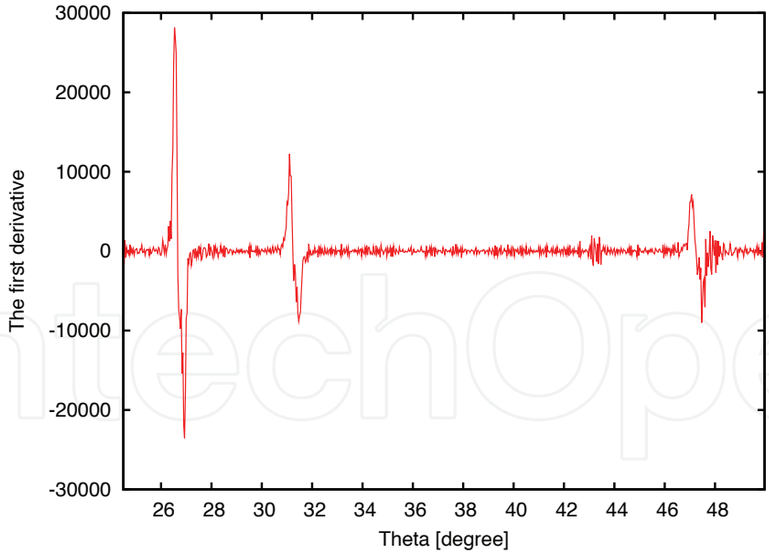


Fig. 3. The first derivative for the computed signal obtained through Fourier synthesis

2.4 Application of the trigonometric polynomial in the integration of partial differential equations

One of the most important roles of the trigonometric polynomial is that played in the solving of the partial differential equations. The first example of this procedure is

applied to the heat equation in one dimensional space in the conditions of the following problem:

$$\begin{cases} \dfrac{\partial u}{\partial t} = a^2 \dfrac{\partial^2 u}{\partial x^2} \\ u(0,t) = u(L,t) = 0 \text{ (boundary condition)} \\ u(x,t) = g(x) \text{ (intial condition)} \end{cases} \tag{23}$$

where a^2 is the diffusion coefficient, it represents the heat conductibility of the material expressed in cm^2/s. The solution of (23) is obtained using the separation of variables and the Fourier series technique. The solution has the form

$$u(t,x) = \sum_{n=1}^{\infty} B_n(t) \sin \frac{n\pi x}{L} \tag{24}$$

where B_n are determined using the Fourier series technique.

$$B_n(t) = \frac{2}{L} \int_0^L u(x,t) \sin \frac{n\pi x}{L} dx \tag{25}$$

Replacing (24) in the heat equation is obtained

$$B_n^{'}(t) + \left(\frac{n\pi a}{L} \right)^2 B_n(t) = 0, \quad n = 0,1,2,\cdots \tag{26}$$

From the initial condition is obtained

$$b_n = B_n(0) = \frac{2}{L} \int_0^L u(x,0) \sin \frac{n\pi x}{L} dx \quad n = 0,1,2,\cdots \tag{27}$$

The relation (27) shows that the right member represents the n Fourier coefficient for the function that gives initial temperature g. By solving the ordinary differential equation (26) is obtained

$$B_n(t) = b_n \exp\left(\left(-n\pi a / L \right)^2 t \right) \quad n = 0,1,2,\cdots \tag{28}$$

Replacing (28) in (24), the general solution of the problem (23) for the heat equation is

$$u(t,x) = \sum_{n=1}^{\infty} b_n \exp\left(-\left(\frac{n\pi a}{L} \right)^2 t \right) \sin \frac{n\pi x}{L} \tag{29}$$

where the gaussian part plays the role of damping factor.

Let consider, as the second example, a vibrating string of length L fixed on both ended in the absence of any external force, $0 \le x \le L$ and $t>0$, its motion is describes by the wave equation

$$\begin{cases} \dfrac{\partial^2 y}{\partial t^2} = c^2 \dfrac{\partial^2 y}{\partial x^2} \\ y(0,t) = y(L,t) = 0 \quad \text{(boundary condition)} \\ y(x,0) = f(x) \quad \text{(initial conditions)} \\ \dfrac{\partial y}{\partial t}(x,0) = g(t) \end{cases} \tag{30}$$

The function y represents the position of each oscillating point versus Ox axis. The function f describes the initial string position and g describes the initial speed of the string. The constant c^2 represents the ratio between straining force and the linear density of the string; the force has the same direction as the movement of the string element. The solution for the problem (30) is obtained using the same technique as in the case of the heat equation and it has the form

$$y(x,t) = \sum_{n=1}^{\infty} \left[a_n \cos\left(nc\pi t / L\right) + b_n t \operatorname{sinc}(nct/L) \right] \sin\frac{n\pi x}{L} \tag{31}$$

where "sinc" represents the normalized sinc function, $a_n = B_n(0) = \dfrac{2}{L}\int_0^L f(x)\sin\dfrac{n\pi x}{L}dx$ and

$b_n = B_n^{'}(0) = \dfrac{2}{L}\int_0^L g(x)\sin\dfrac{n\pi x}{L}dx$ for all $n = 0,1,2,\ldots$

Schrödinger equation is the other example presented that describes the quantum behavior in time and space of a particle with m mass inside the potential V and it is given by

$$i\hbar\frac{\partial \Psi}{\partial t} = -\frac{\hbar^2}{2m}\frac{\partial^2 \Psi}{\partial x^2} + V(x)\Psi \tag{32}$$

where $\hbar$ is Planck constant divided by 2π. If the potential energy is vanished the previous equation becomes the free particle equation and this case will be analyzed forward.

$$\begin{cases} i\hbar\dfrac{\partial \Psi}{\partial t} = -\dfrac{\hbar^2}{2m}\dfrac{\partial^2 \Psi}{\partial x^2} \\ \Psi(0,t) = \Psi(L,t) = 0 \\ \Psi(x,0) = f(x) \end{cases} \tag{33}$$

From physical point of view Ψ represents a probability density generator and $|\Psi|^2 = \Psi\Psi^*$ describes the existence probability of a particle of mass m at position x and time t, thus

$$\|\Psi\|^2 = \int_0^L |\Psi(x,t)|^2 dx = 1 \tag{34}$$

Analogous with the previous two examples the solution of the problem (33) is given by

$$\Psi(x,t)=\sum_{n=1}^{\infty}\exp\left[-\frac{i\hbar}{2m}\left(\frac{n\pi}{L}\right)^2 t\right]c_n\sin\frac{nx\pi}{L}. \tag{35}$$

where $C_n(0)=c_n$, $n=0,\pm1,\pm2,\cdots$ and

$$C_n(t)=\frac{2}{L}\int_0^L\Psi(x,t)\sin\frac{nx\pi}{L}\mathrm{dx} \tag{36}$$

3. Generalization of the Fourier series for the function of infinite period

In the physical and chemical signals analyzing it is often find a non periodical signals defined on the whole real axis. There are many examples in the physics spectroscopy where the signals damp in time due in principal by the absorption process thus there can not be modeled by the periodical functions. The nuclear magnetic resonance (NMR), Fourier transform infrared spectroscopy (FTIR) as well as X-ray absorption spectroscopy (XAS) dedicated to K or L near and extended edges are based on non periodical signals analysis.

3.1 Mathematical background of the discreet and inverse Fourier transform

Let consider the complex form of the Fourier series for a signal *h* defined on the interval $[-T/2,T/2]$ it will be introduced the Fourier transform of *h* based on the concept of infinite period ($T\to\infty$)

$$h(t)=\frac{1}{T}\sum_{n=-\infty}^{\infty}\underbrace{\left\{\int_{-T/2}^{T/2}h(s)\exp\left(-2\pi i\frac{n}{T}s\right)ds\right\}}_{\text{Fourier coefficients}}\exp\left(2\pi i\frac{n}{T}t\right) \tag{37}$$

where the fundamental frequencies f_0 is expressed by $f_0=1/T$. If it be denoted by $f_n=n/T$ and $\Delta f=f_{n+1}-f_n=1/T$ then the relation (37) becomes

$$h(t)=\sum_{n=-\infty}^{\infty}\left\{\int_{-T/2}^{T/2}h(s)\exp\left(-2\pi i f_n s\right)ds\right\}\exp\left(2\pi i f_n t\right)\Delta f \tag{38}$$

If $\Delta f\to 0$ then period *T* goes to infinity and

$$h(t)=\int_{-\infty}^{\infty}\underbrace{\left\{\int_{-\infty}^{\infty}h(s)\exp\left(-2\pi i f s\right)ds\right\}}_{H(f)}\exp\left(2\pi i f t\right)df \tag{39}$$

The function *h* will be found in the scientific literature named as the Fourier integral (Brigham, 1988) and the expression

$$H(f)=\int_{-\infty}^{\infty}h(s)\exp\left(-2\pi i f s\right)ds \tag{40}$$

represents the Fourier transform of the function *h*. From the relation (40) is it possible to obtain the function *h* by inverse Fourier transform given by

$$h(t)=\int_{-\infty}^{\infty}H(f)\exp\left(2\pi i f t\right)df \tag{41}$$

The argument of the exponential function from relation (40) is dimensionless. From physical point of view this is very important to emphasize it. For instance, if the argument represents time [s] or distance [m] thus the argument of Fourier transform has dimension [1/s] and [1/m], therefore the product of dimensions for the arguments of Fourier transform is dimensionless.

From physical point of view the difference between the Fourier series and the Fourier transform is illustrated considering two signals one periodic, *g*, and the other non periodic, *h*. The non periodical signal, *h*, is often find in NMR spectroscopy.

$$g(t)=\begin{cases}0, & \text{if } t<0\\ a\exp(-\gamma t/2)\exp(2\pi i f_0 t), & \text{if } (n\text{-}1)\,\mathrm{T}\le t\le nT,\quad n=1,2,\cdots;\gamma>0\end{cases} \tag{42}$$

$$h(t)=\begin{cases}0, & \text{if } t<0\\ a\exp(-\gamma t/2)\exp(2\pi i f_0 t), & \text{if } t\ge 0,\ \gamma>0\end{cases} \tag{43}$$

The Fourier coefficients A_n and theirs magnitudes associated with periodical signal (42) are given by relation

$$A_n=a\frac{\exp\left(-\frac{\gamma}{2f_0}\right)-1}{2\pi i f_0(1-n)-\frac{\gamma}{2}}\ \text{and}\ |A_n|^2=a^2\frac{\left(\exp\left(-\frac{\gamma}{2f_0}\right)-1\right)^2}{4\pi^2 f_0{}^2(1-n)^2+\frac{\gamma^2}{4}} \tag{44}$$

Fig. 4. shows the graphic for the real part of the periodical *g* signal for a=10, γ=5 ms^{-1} and f_0=2 KHz.

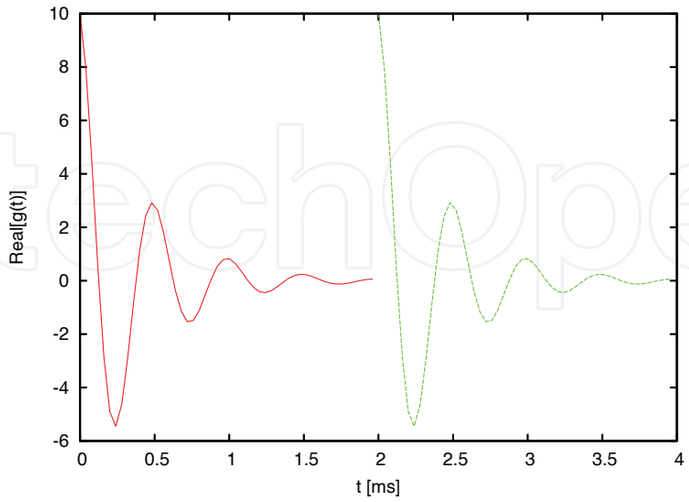


Fig. 4. The periodical physical signal *g*

Fig. 5 represents the spectral distribution of *g* signal that it is defined by the square magnitude of the Fourier coefficients.

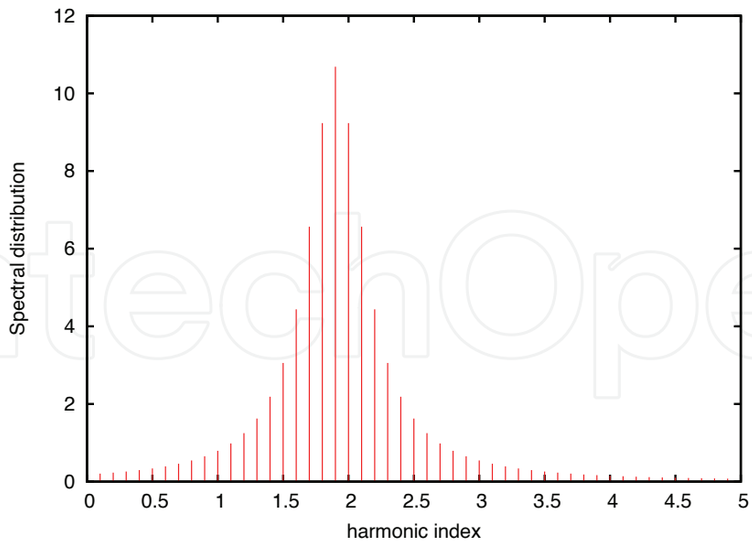


Fig. 5. The spectral distribution of the signal g

The real component of the function (43) is represented in Fig. 6 and the square magnitude of the Fourier transform is given by relation (45) and it is represented in Fig. 7.

$$\left|H(f)\right|^2 = \frac{a^2}{4\pi^2(f_0 - f)^2 + \frac{\gamma^2}{4}} \tag{45}$$

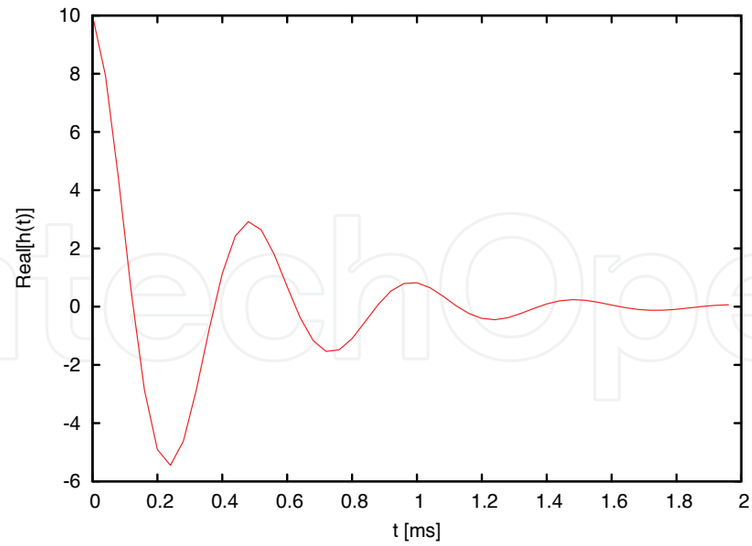


Fig. 6. The real part of non periodical signal h

The maximum value for the spectral distribution take place when $f = f_0$, thus $\left|H_{\max}(f)\right|^2 = 4a^2/\gamma^2$. The full width at half maxim (FWHM) is denoted by $\Delta f_{1/2}$ and $\Delta f_{1/2} = \gamma/2\pi$

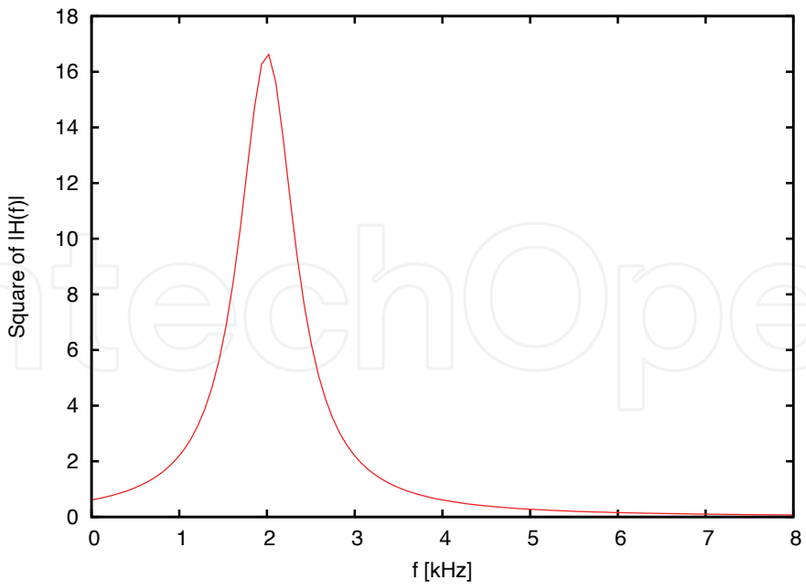


Fig. 7. The square magnitude of Fourier transform of the signal *h*

Some times in signals analysis theory, the inverse of the damping parameter γ is named the relaxation time denoted by τ. Between the relaxation time and FWHM there is the relation $\tau \Delta f_{1/2} = \frac{1}{2\pi}$.

From physical reason it is easier to analyze the resonant answer of a physical signal than free damping oscillations. In NMR spectroscoply this signal is known as Free Impulse Decay (FID). Studying the resonant answer it is possible to obtain the relaxation time parameter of the free oscillations. The relaxation time derives from the width of the spectrum obtained from the Fourier transform of the FID. Therefore it is easier to determine the relaxation time from Fourier transform of *h* signal instead of fit technique applied to FID.

Above it was shown that the Fourier series of periodical signal is represented as a sum of periodical functions with discreet frequencies f_0, $2f_0$, $3f_0$, … as shown in Fig. 5. The amplitudes of the signals associated to each frequency are given by the spectral distribution named Fourier analysis. The difference between Fourier series and Fourier transform is that the latter has the frequencies as argument which continuously varies. Whereas Fourier transform of the signal *h* allows spectral decomposition of it with frequencies defined on the whole real axis.

3.2 The Fourier transform for discreet signals

In practice the function *h* represents a physical signal resulted from an experiment. The signal can be discretizated on *N* samples with a constant step Δt. From physical reasons, the experimental signals can not be acquisitioned on the entire real axis thus the working interval is $\left[-N\Delta t/2,(N/2-1)\Delta t\right]$ (Mandal & Asif, 2007). Instead of the function *H* there are a set of pairs $(n\Delta f, H_n)$, $n=\overline{0,N-1}$ where Δf represents the discretization step of data. Let consider the following relation between discretization steps

$$\Delta f = \frac{1}{N\Delta t} \tag{46}$$

the Fourier transform associated to the set $\left(h(k\Delta t)\right)_{k=\overline{-N/2,N/2-1}}$ is contained in the *H* vector with the components

$$H(n\Delta f) = \Delta t \sum_{k=-N/2}^{N/2-1} h(k\Delta t)\exp\left(-\frac{2\pi ikn}{N}\right), \quad n = \overline{0, N-1}. \tag{47}$$

It is more convenient, for the computation, if all the indexes are positive, for this it is assumed that $q = k + N$ for $k<0$. Relation (47) becomes

$$H(n\Delta f) = \Delta t \sum_{k=0}^{N-1} h(k\Delta t)\exp\left(-\frac{2\pi ikn}{N}\right). \tag{48}$$

Using the same consideration, the inverse Fourier transform has the form

$$h(n\Delta f) = \Delta f \sum_{k=0}^{N-1} \underbrace{\left[\mathrm{Re}\, H(k\Delta f) + i\,\mathrm{Im}\, H(k\Delta f)\right]}_{H(k\Delta f)} \exp\left(\frac{2\pi ikn}{N}\right) \tag{49}$$

If the physical signal is recorded on negative arguments then for the numerical computation of the Fourier transform for the components $(k\Delta t, h_k)$, $k = \overline{-N/2 \ldots N/2-1}$ must be arrange in the following order

$$\begin{gathered}(0,1,2,\cdots,N/2-1) \to (h_0, h_1, h_2, \cdots, h_{N/2-1}) \\ \left(\frac{N}{2}, \frac{N}{2}+1, \frac{N}{2}+2, \cdots, N-1\right) \to (h_{-N/2}, h_{-N/2+1}, h_{-N/2+2}, \cdots, h_{-1}).\end{gathered} \tag{50}$$

3.3 The main algorithms for the Fourier transform. The Filon quadrature and the Cooley-Tukey method

Most of the times the physical-chemical signals can not be expressed analytical, thus it is impossible to use the relation (40). Therefore in computation is used the discreet form of Fourier transform given by the relation (48). Generally speaking the physical signals are recorded around thousands of points; additionally the Fourier transform of the signal is important to compute on the same numbers. By using relation (48) the computation time is too long. This problem was solved by Cooley Tukey algorithm (Brigham, 1988) named in the literature as a Fast Fourier Transform (FFT) method. In the case when the physical signal is registered from pairs in a range of hundreds up to few thousand values can be successfully used the Filon algorithm (Abramowitz & Stegun, 1972). The method assumes that the physical signal is defined on the interval $\left[t_0, t_{2n}\right]$ with step Δt then the real component of the Fourier transform is approximated by

$$\begin{aligned}\int_{t_0}^{t_{2n}} h(t)\cos(2\pi tf)dt \approx{}& \Delta t\,\alpha(2\pi f\Delta t)h_{2n}\sin(2\pi t_{2n}f) - \\ &- \Delta t\left[h_0\sin(2\pi t_0 f) - \beta(2\pi f\Delta t)C_{2n} - \gamma(2\pi f\Delta t)C_{2n-1}\right]\end{aligned} \tag{51}$$

where

$$C_{2n} = \sum_{j=0}^{n} h_{2j}\cos(2\pi f t_{2j}) - \frac{1}{2}\left[h_{2n}\cos(2\pi f t_{2n}) + h_0\cos(2\pi f t_0)\right]$$
$$C_{2n-1} = \sum_{j=0}^{n} h_{2j-1}\cos(2\pi f t_{2j-1}), \quad \alpha(\theta) = \frac{1}{\theta} + \frac{\sin 2\theta}{2\theta^2} - \frac{2\sin^2\theta}{2\theta^3} \tag{52}$$
$$\beta(\theta) = 2\left(\frac{1+\cos^2\theta}{\theta^2} - \frac{\sin 2\theta}{\theta^3}\right), \quad \gamma(\theta) = 4\left(\frac{\sin\theta}{\theta^3} - \frac{\cos\theta}{\theta^2}\right)$$

and the imaginary component of the Fourier transform is given by

$$\int_{t_0}^{t_{2n}} h(t)\sin(2\pi t f)dt \approx \Delta t\,\alpha(2\pi f \Delta t)h_0\cos(2\pi t_0 f) - \\ -\Delta t\left[h_{2n}\cos(2\pi t_{2n} f) - \beta(2\pi f \Delta t)S_{2n} - \gamma(2\pi f \Delta t)S_{2n-1}\right] \tag{53}$$

where

$$S_{2n} = \sum_{j=0}^{n} h_{2j}\sin(2\pi f t_{2j}) - \frac{1}{2}\left[h_{2n}\sin(2\pi f t_{2n}) + h_0\sin(2\pi f t_0)\right]$$
$$S_{2n-1} = \sum_{j=0}^{n} h_{2j-1}\sin(2\pi f t_{2j-1}). \tag{54}$$

By taking into account the relation (46) used in the FFT method it is not possible to compute the Fourier transform for all value of the frequency. This disadvantage can lead to poor resolution of the Fourier transform *H*. Meanwhile the Filon algorithm is more time consuming but its application offers a more reliable resolution. A detailed analysis of these algorithms applied in the extended X-ray absorption fine structure (EXAFS) spectroscopy can be found in the paper (Aldea & Pintea, 2009).

3.4 Application of the Fourier transform in X-ray absorption spectroscopy and X-ray diffraction

The study of XAS can yield electronic and structural information about the local environment around a specific atomic constituent in the amorphous materials (Kolobov et al., 2005),

Additional, this method provides information about the location and chemical state of any catalytic atom on any support (Miller et al., 2006) as well as the nanoparticle of transition metal oxides (Chen et al., 2002; Turcu et al., 2004)). X-ray absorption near edge structure (XANES) is sensitive to local geometries and electronic structure of atoms that constitute the nanoparticles. The changes of the coordination geometry and the oxidation state upon decreasing the crystallite size and the interaction with molecules absorbed on nanoparticles surface can be extracted from XANES spectrum.

The EXAFS is a specific element of the scattering technique in which a core electron ejected by an X-ray photon probes the local environment of the absorbing atom. The ejected

photoelectron backscattered by the neighboring atoms around the absorbing atom interferes constructively with the outgoing electron wave, depending on the energy of the photoelectron. The energy of the photoelectron is equal to the difference between the X-ray energy photon and a threshold energy associated with the ejection of the electron.

X-ray diffraction (XRD) line broadening investigations of nanostructured materials have been limited to find the average crystallite size from the integral breadth or the FWHM of the diffraction profile. In the case of nanostructured materials due to the difficulty of performing satisfactory intensity measurements on the higher order reflections, it is impossible to obtain two orders of (hkl) profile. Consequently, it is not possible to apply the classical method of Warren and Averbach (Warren, 1990). On the other hand we developed a rigorous analysis of the X-ray line profile (XRLP) in terms of Fourier transform where zero strains assumption is not required. The apparatus employed in a measurement generally affects the obtained data and a considerable amount of work has been done to make resolution corrections. In the case of XRLP, the convolution of true data function by the instrumental function produced by a well-annealed sample is described by Fredholm integral equation of the first kind (Aldea et al., 2005; Aldea & Turcu, 2009). A rigorous way for solving this equation is Stokes method based on Fourier transform technique. The local and global structure of nanosized nickel crystallites were determined from EXAFS and XRD analysis.

3.4.1 EXAFS analysis

The interference between the outgoing and the backscattered electron waves has the effect of modulating the X-ray absorption coefficient. The EXAFS function $\chi(k)$ is defined in terms of the atomic absorption coefficient by

$$\chi(k) = \frac{\mu(k) - \mu_0(k)}{\mu_0(k)} \tag{55}$$

where k is the electron wave vector, $\mu(k)$ refers to the absorption by an atom from the material of interest and $\mu_0(k)$ refers to the atom in the free state. The theories of the EXAFS based on the single scattering approximation of the ejected photoelectron by atoms in the immediate vicinity of the absorbing atom gives an expression for $\chi(k)$

$$\chi(k) = \sum_j A_j(k) \sin\left[2kr_j + \delta_j(k)\right] \tag{56}$$

where the summation extends over j coordination shell, r_j is the radial distance from the j^{th} shell and $\delta_j(k)$ is the total phase shift function. The amplitude function $A_j(k)$ is given by

$$A_j(k) = \left(\frac{N_j}{kr_j^2}\right) F(k, r_j, \pi) \exp\left(-2\left(r_j / \lambda_j(k) - k^2\sigma_j^2\right)\right) \tag{57}$$

In this expression N_j is the number of atoms in the j^{th} shell, σ_j is the root mean squares deviation of distance about r_j, $F(k, r_j, \pi)$ is the backscattering amplitude and $\lambda_j(k)$ is the mean free path function for the inelastic scattering. The backscattering factor and the phase shift depend on the kind of atom responsible for scattering and its coordination shell (Aldea et al., 2007). The analysis of EXAFS data for obtaining structural information [N_j, r_j, σ_j, $\lambda_j(k)$]

generally proceeds by the use of the Fourier transform. From $\chi(k)$, the radial structure function (RSF) can be derived. The single shell may be isolated by Fourier transform,

$$\Phi(r) = \int_{-\infty}^{\infty} k^n \chi(k) WF(k) \exp(-2ikr) dk. \tag{58}$$

The EXAFS signal is weighted by k^n (n=1, 2, 3) to get the distribution function of atom distances. Different apodization windows WF(k) are available as Kaiser, Hanning or Gauss filters. An inverse Fourier transform of the RSF can be obtained for any coordination shell,

$$\chi_j(k) = \frac{1}{k^n} WF(k) \int_{R_{1j}}^{R_{2j}} \Phi(r) \exp(2ikr) dr. \tag{59}$$

The theoretical equation for $\chi_j(k)$ function is given by:

$$\chi_j(k) = A_j(k) \sin\left[2kr_j + \delta_j(k)\right], \tag{60}$$

where the index j refers to the jth coordination shell. The structural parameters for the first coordination shell are determined by fitting the theoretical function $\chi_j(k)$ given by the relation (60) with the experimental signal $\chi_j(k)$ derived from relation (59). In the empirical EXAFS calculation, $F(k,r,\pi)$ and $\delta_j(k)$ are conveniently parameterized (Aldea et al., 2007). Eight coefficients are introduced for each shell:

$$F_s(k,r,\pi) = c_0 \left[\exp(c_1 k + c_2 k^2)\right] / k^{c_3} \tag{61}$$

$$\delta_s(k) = a_{-1} k^{-1} + a_0 + a_1 k + a_2 k^2 \tag{62}$$

The coefficients c_0, c_1, c_2, c_3, a_{-1}, a_0, a_1 and a_2 are derived from the EXAFS spectrum of a compound whose structure is accurately known. The values N_s and r_s for each coordination shell for the standard sample are known. The trial values of the eight coefficients can be calculated by algebraic consideration and then they are varied until the fit between the observed and calculated EXAFS is optimized.

3.4.2 XRD analysis

X-ray diffraction pattern of a crystal can be described in terms of scattering intensity as function of scattering direction defined by the scattering angle 2θ, or by the scattering parameter $s = (2\sin\theta)/\lambda$, where λ is the wavelength of the incident radiation. It is discussed the X-ray diffraction for the mosaic structure model in which the atoms are arranged in blocks, each block itself being an ideal crystal, but with adjacent blocks not accurately fitted together. The experimental XRLP, h, represents the convolution between the true sample f and the instrumental function g

$$h(s) = \int_{-\infty}^{+\infty} g(s - s^*) f(s^*) \, ds^* \tag{63}$$

The equation (63) is equivalent with the following relation

$$H(L) = G(L) F(L), \tag{64}$$

where $F(L)$, $H(L)$ and $G(L)$ are the Fourier transforms of the true sample, experimental XRLP and instrumental function, respectively. The variable L is the perpendicular distance to the (hkl) reflection planes. The generalized Fermi function (GFF) (Aldea et al., 2000) is a simple function with a minimal number of parameters, suitable for the XRLP global approximation based on minimization methods and it is defined by relation:

$$h(s) = \frac{A}{e^{a(s-c)} + e^{-b(s-c)}}, \tag{65}$$

where A, a, b, c are unknown parameters. The values A, c describe the amplitude, the position of the XRLP and a, b control its shape. In the case when X-ray line profiles h and g are approximated by GFF distribution then the solution of Fedholm integral equation of the first kind represents the true sample function and it is given by

$$f(s) = \frac{2A_h\rho_g}{\pi A_g} \frac{\cos\frac{\pi\rho_h}{2\rho_g}\cosh\rho_h s}{\cos\frac{\pi\rho_h}{\rho_g} + \cos 2\rho_h s} \tag{66}$$

where the arguments of trigonometric and hyperbolic functions depend on the shape parameters of the h, g signals, respectively. They are expressed by $\rho_h = (a_h + b_h)/2$ and $\rho_g = (a_g + b_g)/2$.

3.4.3 EXAFS results

The extraction of the EXAFS signal is based on the threshold energy of the nickel K edge determination followed by background removal of pre-edge and after-edge base line fitting with different possible modeling functions where $\mu_0(k)$ and $\mu(k)$ evaluation are presented in Fig. 8.

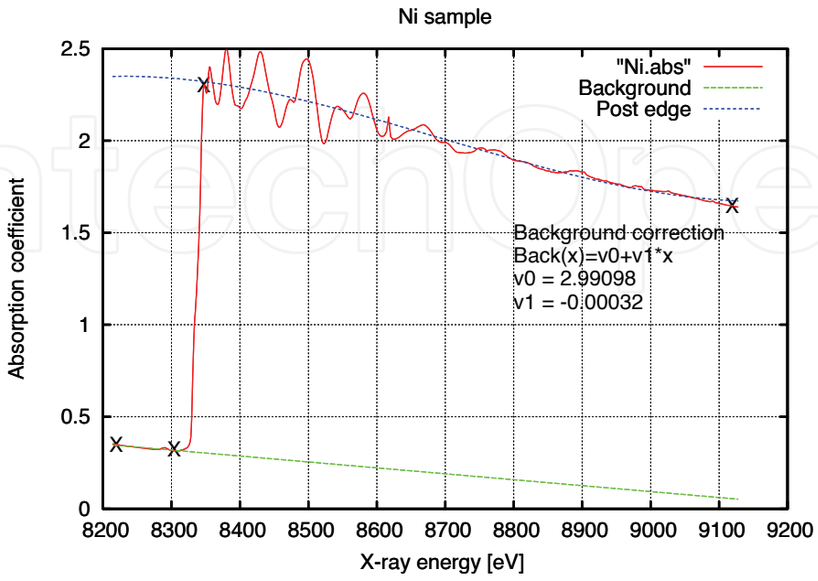


Fig. 8. The absorption coefficient of the nickel K edge

In according with relation (55) EXAFS signals modulated by Hanning and Gauss filters were performed in the range 2 Å -14 Å and they are shown in Fig. 9. In order to obtain the atomic distances distribution it was computed the RSF, using the relation (58) and the Filon algorithm.

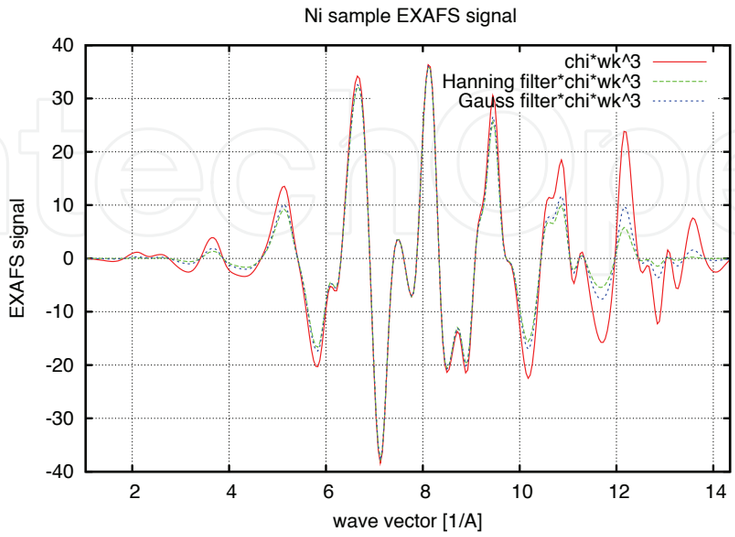


Fig. 9. EXAFS signal for the nickel crystallites

The mean Ni-Ni distances of the first coordination shell for standard sample at room temperature are closed to values of R_1=2.49Å. Based on relation (46) between Δk and Δr steps, the computation of the RSF using the FFT of the EXAFS signal gives a non reliable resolution. To avoid this disadvantage it used the Filon algorithm for Fourier transform procedure. Based on this procedure the Fourier transform of $k^3\chi(k)WF(k)$, performed in the range 0.51 Å and 2.79 Å, are shown in Fig. 10 for the standard Ni foil investigation. In order to minimize the spurious errors in the RSF it was considered Gauss filter as the window function.

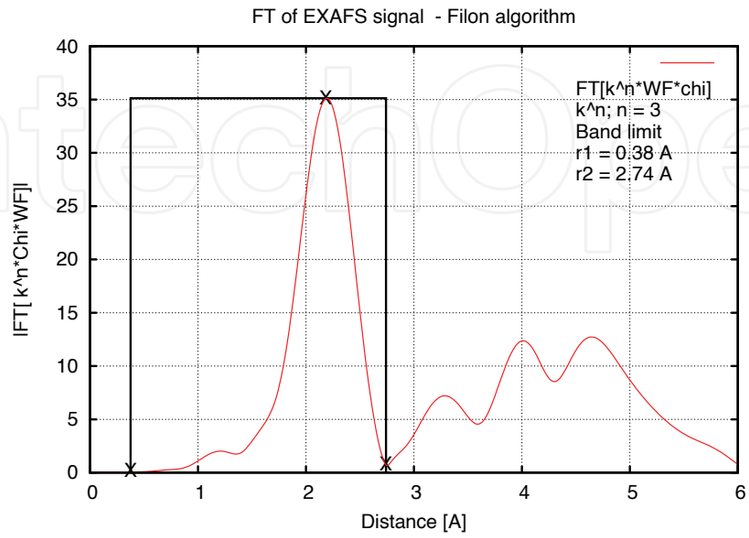


Fig. 10. The Fourier transform of the EXAFS spectrum for the nickel foil

Each peak from $|\Phi(r)|$ is shifted from the true distance due to the phase shift function that is included in the EXAFS signal. We proceed by taking the inverse Fourier transform given by relation (59) of the first neighboring peak, and then extracting the amplitude function $A_j(k)$ and the phase shift function $\delta(k)$ in according with the relations (61) and (62).

By Lavenberg-Marquard fit applied to the relation (60) and from the experimental contribution for each coordination shell, are evaluated the interatomic distances, the number of neighbors

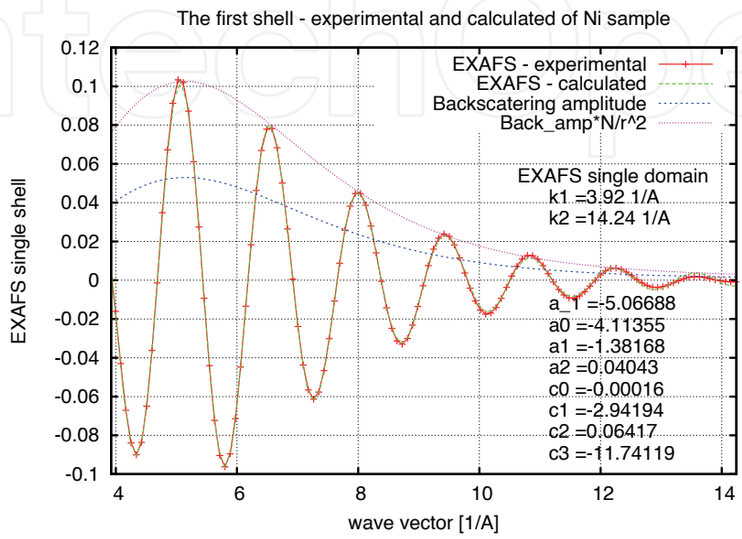


Fig. 11. Experimental and calculated EXAFS signals of the first coordination shell of the nickel foil

and the edge position. Fig. 11 shows the calculated and the experimental EXAFS functions $\chi_1(k)$ of the first shell for the investigated sample.

3.4.4 XRD results

Practically speaking, however, it is not easy to obtain accurate values of the crystallite size and the microstrain without extreme care in the experimental measurements and analysis of XRD data. The Fourier analysis of XRLP validity depends strongly on the magnitude and the nature of the errors propagated in the data analysis. In paper (Aldea et al., 2000) are treated three systematic errors: the uncorrected constant background, the truncation and the effect of the sampling for the observed profile at a finite number of points that appear in discrete Fourier analysis. In order to minimize propagation of these systematic errors, a global approximation of the XRLP is adopted instead of the discrete calculations. Therefore, the analysis of the diffraction line broadening in X-ray powder pattern was analytically calculated using the GFF facilities.

The reason of this choice, as described above, was simplicity and the mathematical elegance of the analytical Fourier transform magnitude and the integral width of the true XRLP. The robustness of the GFF approximation for the XRLP arises from possibility of using the analytical form of the Fourier transform instead of the numerical FFT. The validity of the microstructural parameters are closely related to accuracy of the Fourier transform magnitude of the true XRLP. The experimental relative intensities with respect to θ values

and the nickel foil as instrumental broadening effect are shown in Fig. 12. The next steps consist in the background correction of the XRLP by the polynomial procedures and the determination of the best parameters of GFF distributions by nonlinear least squares fit. In order to determine the average crystallite size, the lattice microstrain and the probability of defects were computed the true XRLP by the Fourier transform technique and it is illustrated in Fig. 13, the curve is centred on its mass centre s_0.

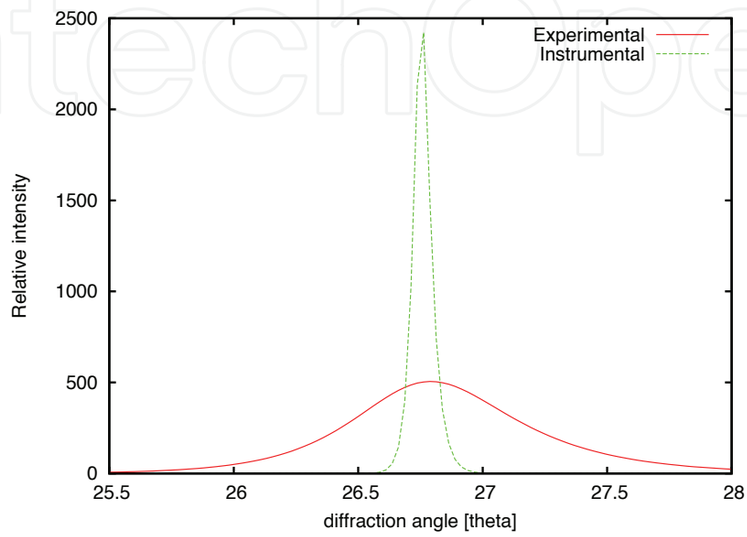


Fig. 12. The experimental XRLP (*h*) and the instrumental signals (*g*)

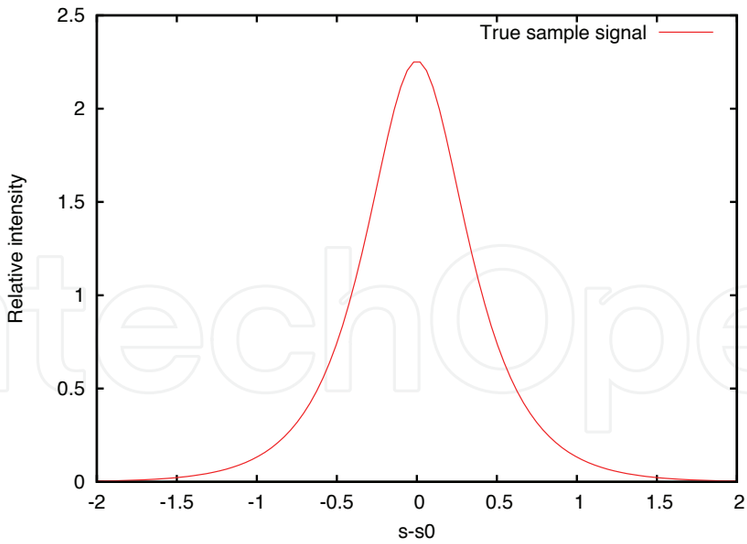


Fig. 13. The true sample signal (*f*)

4. Conclusions

In this contribution it has presented the mathematical background of Fourier series and Fourier transform used in nanomaterials structure field.

The conclusions that can be drawn from this contribution are:

i. The physical periodical signals are successfully modeled using the trigonometric polynomial such us global approximation of the XRLP and the spectral distribution determination based on the Fourier analysis;
ii. The most important tools applied in EXAFS is based on the direct and inverse Fourier transform methods;
iii. The examples presented are based on the original contributions published in the scientific literature.

The experimental data used in analyses consists in measurements that have done to Beijing Synchrotron Radiation Facilities from High Institute of Physics.

5. Acknowledgement

The authors are grateful to Beijing Synchrotron Radiation Facilities staff for beam time and for their technical assistance in XAS and XRD measurements. This work was partially supported by UEFISCDI, projects number 32-119/2008 and 22-098/2008.

Appendix

In this appendix are given the main analytical properties of the Fourier transform.

i. *Linearity*. If the signals x and y have the Fourier transform X and Y then the Fourier transform of $\alpha x + \beta y$ is $\alpha X + \beta Y$.
ii. *Symmetry*. If the Fourier transform of the function h is H, then

$$h(-f) = \int_{-\infty}^{\infty} H(t)\exp\left(-2\pi i f t\right)dt \tag{67}$$

iii. *Scaling*. If h has the Fourier transform H then

$$\int_{-\infty}^{\infty} h(kt)\exp(-2\pi ift)dt = \frac{1}{|k|}H(f/k), \quad k \in R^* \tag{68}$$

iv. *Shifting*. If the Fourier transform of h is H and h is translated with t_0 then

$$\int_{-\infty}^{\infty} h(t-t_0)\exp(-2\pi ift)dt = \exp(-2\pi if t_0)H(f) \tag{69}$$

v. If the signal h_e is even function and the Fourier transform of h_e is H_e then

$$H_e(f) = \int_{-\infty}^{\infty} h_e(t)\cos(2\pi ft)dt \tag{70}$$

vi. If the signal h_o is odd function and the Fourier transform of h_o is H_o then

$$H_o(f) = -i\int_{-\infty}^{\infty} h_o(t)\sin(2\pi ft)dt \tag{71}$$

vii. Any real function defined on a symmetrical interval has the following decomposition

$$h(t) = h_o(t) + h_e(t)\,, \tag{72}$$

thus

$$H(f) = H_o(f) + H_e(f) \tag{73}$$

For the next properties are assuming the function h is sufficiently smooth so that can be acceptable the differentiation and the integration.

viii. The Fourier transform of the derivative of the function h is given by

$$H_{\frac{dh}{dt}}(f) = (2\pi i f)H_h(f) \tag{74}$$

where H_h represents the Fourier Transform of the function h, and for the n times derivative

$$H_{\frac{d^n h}{dt^n}}(f) = (2\pi i f)^n H_h(f) \tag{75}$$

ix. The derivative of the Fourier transform is given by

$$\frac{dH_h(f)}{df} = -2\pi i H_{th}(f) \tag{76}$$

and for the n times derivative of the Fourier transform

$$\frac{d^n H_h(f)}{df^n} = (-2\pi i)^n H_{t^n h}(f) \tag{77}$$

6. References

Abramowitz, M. & Stegun, I. (1972). *Handbook of Mathematical Functions*, Dover Publication, ISBN 0-486-61272-4, NY, USA

Aldea, N. & Indrea, E. (1990). XRLINE, a program to evaluate the crystallite size of supported metal-catalysts by single X-ray profile fourier-analysis. *Computer Physics Communications*, Vol.60, No.1, (August 1990), pp. 155-163, ISSN: 0010-4655

Aldea, N.; Gluhoi, A.; Marginean, P.; Cosma, C. & Yaning X. (2000). Extended X-ray absorption fine structure and X-ray diffraction studies on supported nickel catalysts. *Spectrochimica Acta B*, Vol.55, No.7, (July 2000), pp. 997-1008, ISSN: 0584-8547

Aldea, N.; Barz, B.; Silipas, T. D.; Aldea, F. & Wu, Z. (2005). Mathematical study of metal nanoparticle size determination by single X-ray line profile analysis. *Journal of Optoelectronics and Advanced Materials*, Vol.7, No.6, (December 2005), pp. 3093-3100, ISSN: 1454-4164

Aldea, N.; Marginean, P.; Rednic, V.; Pintea, S.; Barz, B.; Gluhoi, A.; Nieuwenhuys, B. E.; Xie Y.; Aldea, F. & Neumann, M. (2007). Crystalline and electronic structure of gold nanoclusters determined by EXAFS, XRD and XPS methods. *Journal of Optoelectronics and Advanced Materials*, Vol.9, No.5, (May 2007), pp. 1555-1560, ISSN 1454-4164

Aldea, N.; Turcu, R.; Nan, A.; Craciunescu, I; Pana, O; Yaning, X.; Wu, Z.; Bica, D; Vekas, L. & Matei, F. (2009). Investigation of nanostructured Fe_3O_4 polypyrrole core-shell composites by X-ray absorbtion spectroscopy and X-ray diffraction using synchrotron radiation. *Journal of Nanoparticle Research*, Vol.11, No.6, (August 2009), pp. 1429-1439, ISSN: 1388-0764.

Aldea, N.; Pintea, S.; Rednic, V.; Matei, F. & Xie Y. (2009). Comparative study of EXAFS spectra for close-shell systems. *Journal of Optoelectronics and Advanced Materials*, Vol.11, No.12, (December 2009), pp. 2167 – 2171, ISSN: 1454-4164

Bachmann, G.; Narici, L. & Beckenstein, E. (2002). *Fourier and Wavelet Analysis* (2nd edition), Springer, ISBN 978-0-387-98899-3, New York, USA

Brigham, E. (1988). *The Fast Fourier Transform and Its Applications*, Prentice Hall, ISBN 0133075052, New Jersey, USA

Chen, L.X.; Liu, T.; Thurnauer, M.C.; Csencsits, R. & Rajh, T. (2002). Fe_2O_3 nanoparticle structures investigated by X-ray absorption near-edge structure, surface modifications, and model calculations. *Journal of Physical Chemistry B*, Vol.106, No.34, (August 2002), pp. 8539-8546, ISSN 1520-6106.

Kolobov, A. V.; Fons, P.; Tominaga, J.; Frenkel, A. I.; Ankudinov, A. L. & Uruga, T. (2005). Local Structure of Ge-Sb-Te and its modification Upon the Phase Transition. *Journal of Ovonic Research*, Vol.1, No.1, (February 2005), pp. 21 – 24, ISSN 1584 - 9953

Mandal, M & Asif, A. (2007). *Continuous and Discrete Time Signals and Systems,* Cambridge University Press, ISBN 9780521854559, London , UK.

Miller, J.T.; Kropf, A.J.; Zha, Y.; Regalbuto, J.R.; Delannoy, L.; Louis, C.; Bus, E. & Bokhoven, J.A. (2006). The effect of gold particle size on Au{single bond}Au bond length and reactivity toward oxygen in supported catalysts. *Journal of Catalysis*, Vol.240, No.2, (June 2006), pp. 222-234, ISSN: 00219517

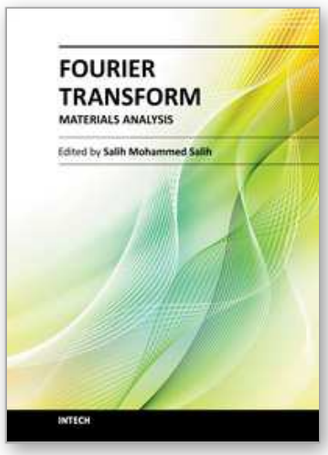
Richard, P.; Leighton, R.B. & Sands M. (2005). *The Feynman Lectures on Physics, Vol. 1: Mainly Mechanics, Radiation, and Heat,* (2nd edition), Addison Wesley, ISBN 978-0805390469, Boston, USA

Tang, K-T. (2007). *Mathematical Methods for Engineers and Scientists 3, Fourier Analysis, Partial Differential Equations and Variational Methods* (vol. 3), Springer-Verlag, ISBN 978-3540446958, Berlin-Heidelberg, Germany

Turcu, R.; Peter, I.; Pana, O.; Giurgiu, L; Aldea, N.; Barz, B.; Grecu, M.N. & Coldea, A. (2004). Structural and magnetic properties of polypyrrole nanocomposites. *Molecular Crystals and Liquid Crystals*, Vol. 417, pp. 719-727, ISSN 1058-725X

Walker, J. (1996). *Fast Fourier Transforms*, (2nd edition), CRC Press, ISBN 978-0849371639, Boca Raton, USA

Warren, B. E. (1990). *X-Ray Diffraction*, Dover Publications, ISBN 0486663175, NY, USA



Fourier Transform - Materials Analysis

Edited by Dr Salih Salih

ISBN 978-953-51-0594-7
Hard cover, 260 pages
Publisher InTech
Published online 23, May, 2012
Published in print edition May, 2012

The field of material analysis has seen explosive growth during the past decades. Almost all the textbooks on materials analysis have a section devoted to the Fourier transform theory. For this reason, the book focuses on the material analysis based on Fourier transform theory. The book chapters are related to FTIR and the other methods used for analyzing different types of materials. It is hoped that this book will provide the background, reference and incentive to encourage further research and results in this area as well as provide tools for practical applications. It provides an applications-oriented approach to materials analysis written primarily for physicist, Chemists, Agriculturalists, Electrical Engineers, Mechanical Engineers, Signal Processing Engineers, and the Academic Researchers and for the Graduate Students who will also find it useful as a reference for their research activities.

How to reference

In order to correctly reference this scholarly work, feel free to copy and paste the following:

Florica Matei and Nicolae Aldea (2012). Fourier Series and Fourier Transform with Applications in Nanomaterials Structure, Fourier Transform - Materials Analysis, Dr Salih Salih (Ed.), ISBN: 978-953-51-0594-7, InTech, Available from: http://www.intechopen.com/books/fourier-transform-materials-analysis/fourier-series-and-fourier-transform-with-applications-in-nanomaterials-structure

INTECH
open science | open minds

InTech Europe
University Campus STeP Ri
Slavka Krautzeka 83/A
51000 Rijeka, Croatia
Phone: +385 (51) 770 447
Fax: +385 (51) 686 166
www.intechopen.com

InTech China
Unit 405, Office Block, Hotel Equatorial Shanghai
No.65, Yan An Road (West), Shanghai, 200040, China
中国上海市延安西路65号上海国际贵都大饭店办公楼405单元
Phone: +86-21-62489820
Fax: +86-21-62489821

© 2012 The Author(s). Licensee IntechOpen. This is an open access article distributed under the terms of the Creative Commons Attribution 3.0 License, which permits unrestricted use, distribution, and reproduction in any medium, provided the original work is properly cited.

IntechOpen

IntechOpen